Available online at www.sciencedirect.com
ScienceDirect
Trans. Nonferrous Met. Soc. China 24(2014) 2796−2804
Transactions of Nonferrous Metals Society of China
www.tnmsc.cn

Hot deformation behavior of as-quenched 7005 aluminum alloy

Ming-liang WANG, Pei-peng JIN, Jin-hui WANG, Li HAN

Qinghai Provincial Key Laboratory of New Light Alloys, School of Mechanical Engineering, Qinghai University, Xining 810016, China

Received 15 August 2013; accepted 5 November 2013

Abstract: The compressive deformation behavior of as-quenched 7005 aluminum alloy was investigated at the temperature ranging from 250 °C to 450 °C and strain rate ranging from 0.0005 s^{-1} to 0.5 s^{-1} on Gleeble−1500 thermal-simulation machine. Experimental results show that the flow stress of as-quenched 7005 alloy is affected by both deformation temperature and strain rate, which can be represented by a Zener−Hollomon parameter in an exponent-type equation. By comparing the calculated flow stress and the measured flow stress, the results show that the calculated flow stress agrees well with the experimental result. Based on a dynamic material model, the processing maps were constructed for the strains of 0.1, 0.3 and 0.5. The maps and microstructural examination revealed that the optimum hot working domain is 270−340 °C, 0.05−0.5 s^{-1} with the reasonable dynamic recrystallization. The instability domain exhibits adiabatic shear bands and flow localization, which should be avoided during hot working in order to obtain satisfactory properties.

Key words: 7005 alloy; hot compression deformation; constitutive equation; processing map

1 Introduction

In view of their high specific strength and excellent mechanical properties, 7000 series aluminum alloys have been widely used as aircraft and vehicles structure components [1,2]. However, the desirable hot workability affected by the strain rate and deformation temperature is one of important reasons for the extensive application of the 7000 series high-strength aluminum alloys. Therefore, a good understanding of high-strength aluminum alloys behavior at hot deformation condition is very important for the designers of metal forming processes (hot extrusion, forging and rolling).

In the past, the hot deformation behavior of 7000 series aluminum alloys was investigated by some researchers. RAJAMUTHAMILSELVAN and RAMANATHAN [3] gained the optimum hot working parameters and the domains of flow instability according to the processing map for 7075 aluminum alloy. LIN et al [4] investigated the effects of strain on the efficiency of power dissipation, instability parameter, processing maps and microstructural evolution for 7075 aluminum alloy, and found that some types of unstable flow manifestation (e. g. adiabatic shear bands or flow localization) occur during hot deformation with the increase of strain. JIN et al [5] investigated the hot deformation behavior of 7015 aluminum alloy during compression at elevated temperatures. They found that some material parameters are sensitive to the deformation temperature and strain rate and developed a Zener−Hollomon parameter in the hyperbolic-sine equation model to represent the peak stress level. ZHEN et al [6] studied the microstructure characteristics of 7050 aluminum alloy after high-temperature compression deformation. The results show that the softening mechanism of 7050 alloy is not sensitive to strain rate, the primary softening mechanism of 7050 alloy deformed at 340, 380 and 420 °C with the strain rate of 0.1 s^{-1} is dynamic recovery. Dynamic recrystallization is the main softening mechanism of the alloy deformed at 460 °C and different strain rates.

Despite large amount of investigation invested into the hot deformation behavior of 7000 series aluminum alloy, there is little research work focusing on the deformation characteristics of 7005 aluminum alloy in quenching condition. The objective of the present work is to analyze the flow stress behavior in terms of strain rate and deformation temperature sensitivities, develop

Foundation item: Project (2011CB612200) supported by the National Basic Research Program of China
Corresponding author: Pei-peng JIN; Tel: +86-971-5363028; E-mail: jinpeipeng@hotmail.com
DOI: 10.1016/S1003-6326(14)63411-7

constitutive equation to describe the dependence of the flow stress on strain rate and temperature and establish processing maps to optimize the hot working parameters for as-quenched 7005 aluminum alloy.

2 Experimental

In the present study, commercial 7005 aluminum alloy was selected as the raw material. Its composition (mass fraction, %) is as follows: 4.6 Zn, 1.5 Mg, 0.1 Cu, 0.6 Mn, 0.2 Cr, 0.07 Si, 0.02 Ti, 0.15 Fe, 0.08 Zr, with the balance Al. The experimental alloys were machined to cylindrical specimens with 10 mm in diameter and 15 mm in height. The samples were solutionized at 535 °C for 4 h and quenched in water at 40−50 °C. The initial microstructure of as-quenched 7005 aluminum alloy is shown in Fig. 1. The average grain diameter was about 400 μm. Hot compression tests were performed on a Gleeble−1500 thermal simulation machine at temperatures of 250, 300, 350, 400 and 450 °C and strain rates of 0.0005, 0.005, 0.05 and 0.5 s^{-1}. Before the compression tests, the specimens were held at testing temperature for 6 min to achieve uniform temperature throughout the bulks. Graphite lubricant was used to reduce friction between the die and specimen. The specimens were compressed to 60% reduction, and quenched in water immediately. The deformed structures were sectioned parallel to the compression axis along the direction of centerline and polished following the standard metallographic specimen preparation procedure and etched with Keller's reagent for the microstructural observations.

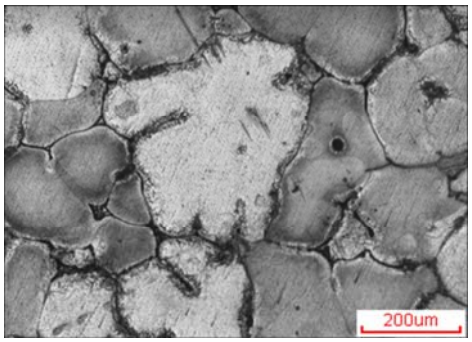

Fig. 1 Initial microstructure of as-quenched 7005 aluminum alloy

3 Results and discussion

3.1 Flow behavior

The load-stroke data were converted into true stress−true strain curves using standard equations. Figure 2 shows the typical true stress−strain curves

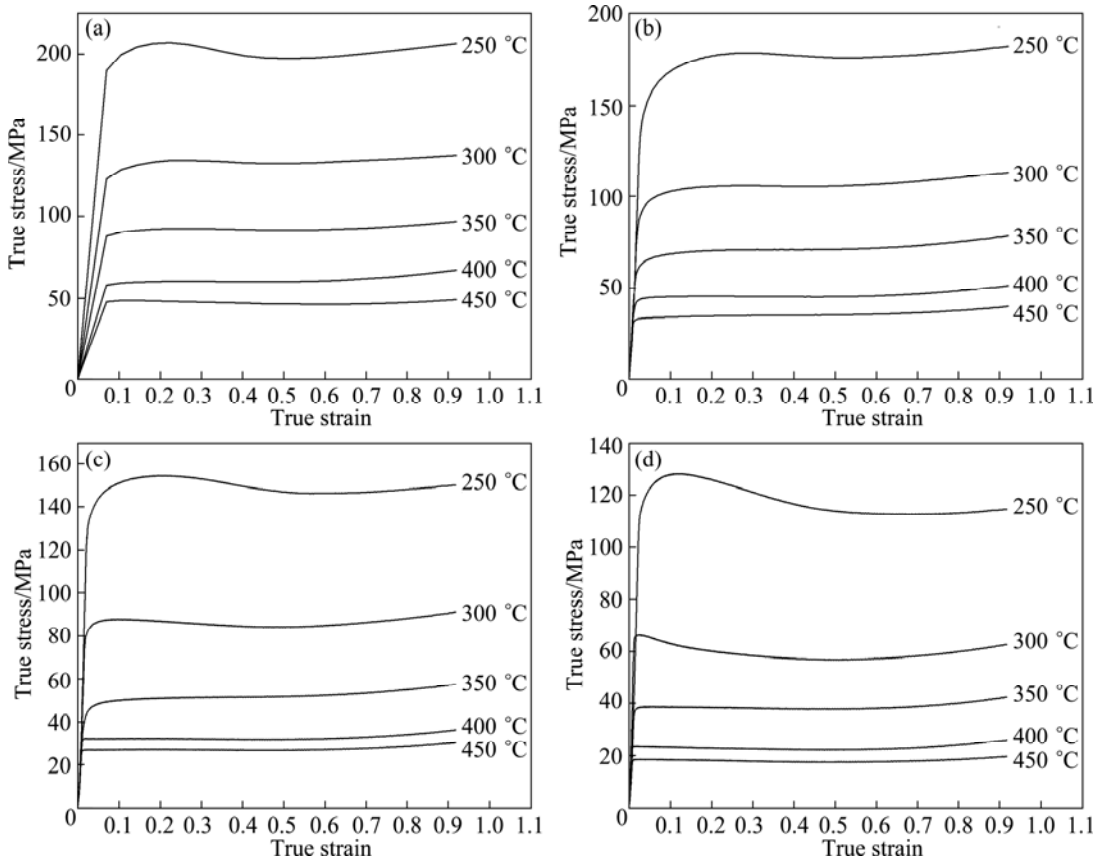

Fig. 2 True stress−true strain curves of as-quenched 7005 aluminum alloy under different strain rates: (a) 0.5 s^{-1}; (b) 0.05 s^{-1}; (c) 0.005 s^{-1}; (d) 0.0005 s^{-1}

obtained from hot compression tests of as-quenched 7005 alloy. As can be seen in Fig. 2, the stress increases sharply in the initial stage of the deformation due to the fact that the work hardening rate is higher than the softening rate. Then, the stress increases at a decreased rate induced by the competition between working hardening and softening (dynamic recovery and dynamic recrystallization); the stress drops when a large number of dislocations rearrange and unlike dislocations counteract. Finally, the stress tends to become steady when the work hardening and softening reach a dynamic equilibrium, then the dislocation density maintains relatively constant.

Obviously, the flow stress was found to depend on deformation temperature and strain rate; the flow stress increases with the decrease of deformation temperature for a given strain rate and increases with the increase of strain rate for a given deformation temperature. The flow stress at a true strain of 0.5 is plotted as a function of deformation temperature in Fig. 3(a), and Fig. 3(b) represents the flow stress at a true strain of 0.5 as a function of the logarithm of strain rate. As can be seen in Fig. 3, the higher the strain rate, the higher the flow stress; while the higher the deformation temperature, the lower the flow stress. Hence, the effects of deformation temperature and strain rate on the flow stress are significant under all the tested conditions.

Generally, the true stress−strain curves articulate the intrinsic relationship of flow stress with thermodynamic behavior. However, it is not appropriate or precise to predict the deformation mechanisms by relying the shape of the flow curves only during hot working [7,8]. Therefore, it is necessary to study the constitutive characteristics and processing maps for as-quenched 7005 aluminum alloy.

3.2 Constitutive equation of flow stress

Generally, the constitutive relation is used as the important factor for the analysis problem of metal-forming process [9−14]. The base equations that are used are usually shown below [15,16]:

$$\dot{\varepsilon} = A_1\sigma^{n_1}\exp\left(-\frac{Q}{RT}\right) \quad (1)$$

$$\dot{\varepsilon} = A_2\exp(\beta\sigma)\exp\left(-\frac{Q}{RT}\right) \quad (2)$$

$$\dot{\varepsilon} = A[\sinh(\alpha\sigma)]^n\exp\left(-\frac{Q}{RT}\right) \quad (3)$$

$$Z = \dot{\varepsilon}\exp\left(\frac{Q}{RT}\right) = A[\sinh(\alpha\sigma)]^n \quad (4)$$

where A_1, A_2, A_3, n_1, α, β and n are material constants; $\dot{\varepsilon}$ is the strain rate; T is the thermodynamic temperature;

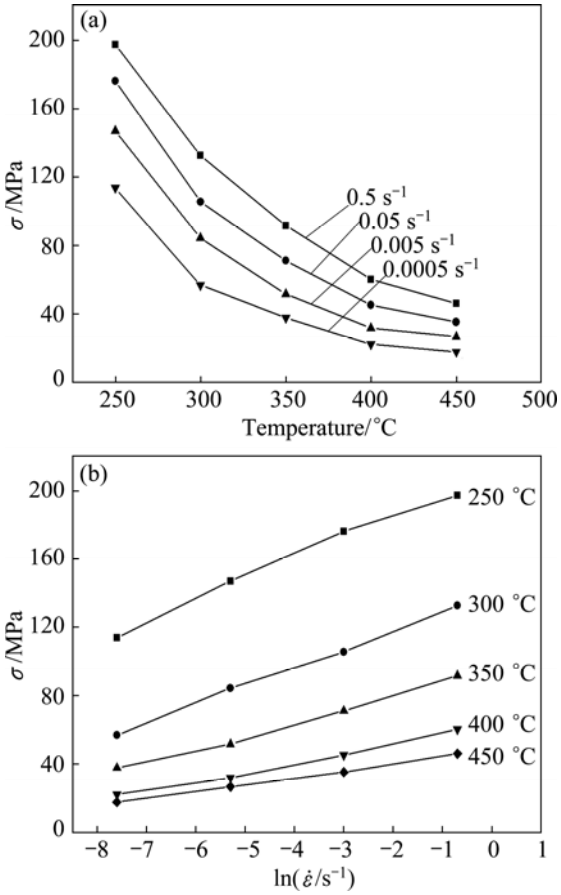

Fig. 3 Effect of deformation parameters on flow stress at true strain of 0.5: (a) Effect of strain rate; (b) Effect of deformation temperature

R is the mole gas constant (8.314 J/(K·mol^{-1})); Q is deformation activation energy; Z is Zener−Hollomon parameter; α is an adjustable constant, $\alpha=\beta/n_1$.

Considering the definition of hyperbolic law, the flow stress, σ, can be written as a function of Zener−Hollomon parameter:

$$\sigma = \frac{1}{\alpha}\ln\left\{\left(\frac{Z}{A}\right)^{1/n} + \left[\left(\frac{Z}{A}\right)^{2/n} + 1\right]^{1/2}\right\} \quad (5)$$

Taking the logarithm of both sides of Eqs. (1) and (2), respectively, gives

$$\ln\dot{\varepsilon} = \ln A_1 - Q/(RT) + n_1\ln\sigma \quad (6)$$

$$\ln\dot{\varepsilon} = \ln A_2 - Q/(RT) + \beta\sigma \quad (7)$$

where σ is the flow stress at the true strain of 0.5. The slope of the plot of $\ln\dot{\varepsilon}$ against $\ln\sigma$ and the slope of the plot of $\ln\dot{\varepsilon}$ against σ can be used for obtaining the values of n_1 and β, respectively, as shown in Fig. 4. Because the slope of these lines is approximately the same, the values of n_1 and β can be obtained for different deformation temperatures by liner fitting method, and the

mean values of n_1 and β can be computed as 8.5834 MPa^{-1} and 0.1458 MPa^{-1}, respectively. Therefore, $\alpha=\beta/n_1=0.01699\ MPa^{-1}$.

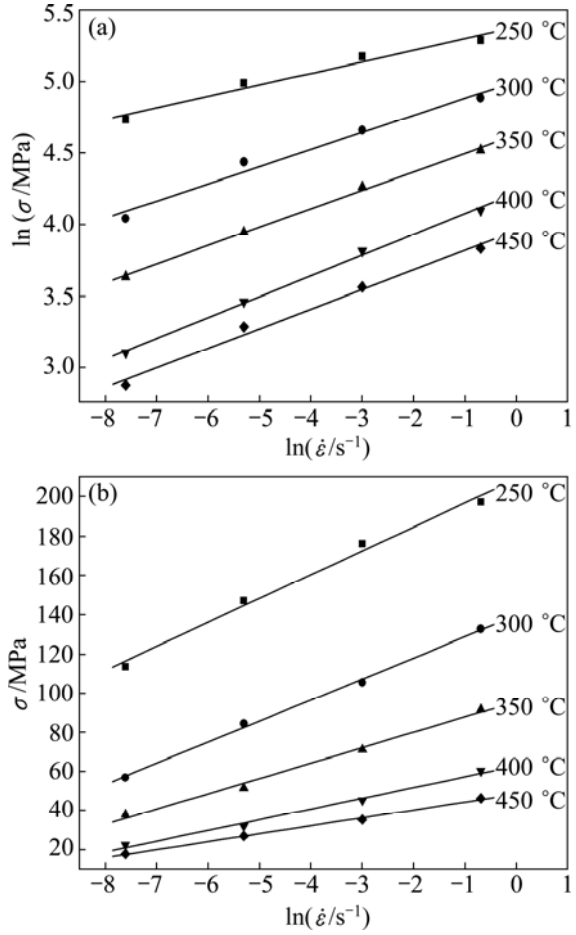

Fig. 4 Relationships between strain rate and flow stress: (a) $\ln\dot{\varepsilon}$ and $\ln\sigma$; (b) $\ln\dot{\varepsilon}$ and σ

By taking natural logarithm from Eq. (3), the following expression can be derived:

$$\ln\dot{\varepsilon}=\ln A+n\ln[\sinh(\alpha\sigma)]-\left(\frac{Q}{RT}\right) \tag{8}$$

The slope of the plot of $\ln\dot{\varepsilon}$ against $\ln[\sinh(\alpha\sigma)]$ can be used for obtaining the value of n, and the plot is shown in Fig. 5.

For the given strain rate conditions, differentiating Eq. (8) gives

$$Q=Rn\left[\frac{\partial\ln[\sinh(\alpha\sigma)]}{\partial(1/T)}\right]_{\dot{\varepsilon}} \tag{9}$$

By substituting the values of temperature and flow stress under different strain rates into Eq. (9), the relationship between $\ln[\sinh(\alpha\sigma)]$ and temperature can be obtained as Fig. 6. Then, the value of Q can be derived from the slope in a plot of $\ln[\sinh(\alpha\sigma)]$ as a function of $1/T$. As can be seen in Fig. 6, four straight lines almost

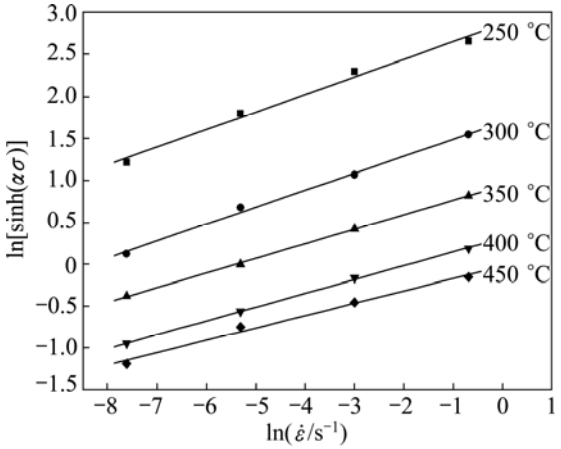

Fig. 5 Relationship between $\ln[\sinh(\alpha\sigma)]$ and $\ln\dot{\varepsilon}$

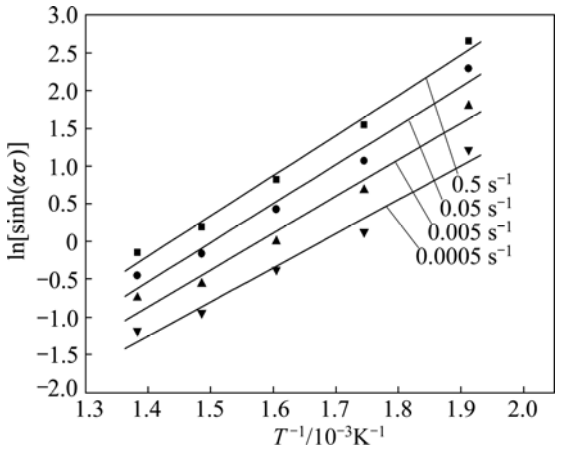

Fig. 6 Relationship between $\ln[\sinh(\alpha\sigma)]$ and temperature

parallel. Hence, the average slope of these four lines from Fig. 6 was solved. Meanwhile, the average slope of these five lines from Fig. 5 for obtaining n was also solved. Therefore, the Q value can be calculated by Eq. (9), and it is 234.51 kJ/mol, the value is higher than that for self-diffusion in Al (142 kJ/mol) [17].

By logarithmic transformation of Eq. (4), the following expression can be expressed as

$$\ln Z=\ln A+n\ln[\sinh(\alpha\sigma)] \tag{10}$$

The relationship between $\ln Z$ and $\ln[\sinh(\alpha\sigma)]$ can be obtained as shown in Fig. 7. From this figure, the values of A and n can be easily obtained as 1.363×10^{17} and 5.526, respectively. The correlation coefficient is 0.99, revealing a good liner relation between $\ln Z$ and $\ln[\sinh(\alpha\sigma)]$. The liner equation can be described as

$$\ln Z=39.454+5.526\ln[\sinh(\alpha\sigma)] \tag{11}$$

Finally, substituting the values of α, n, A and Q into Eq. (3), the flow stress for as-quenched 7005 aluminum alloy during high temperature compression can be represented by a hyperbolic sine equation. The equation can be expressed as follows:

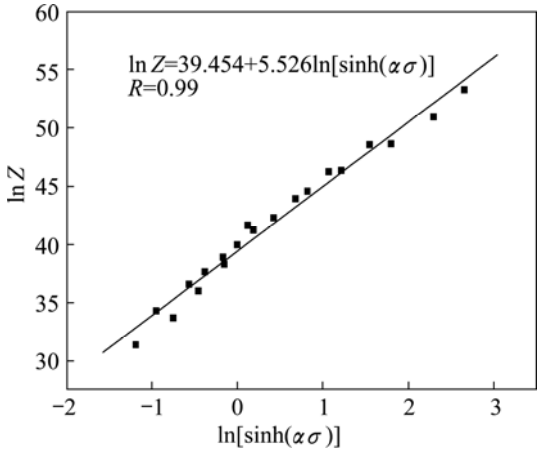

Fig. 7 Relationship between ln Z and ln[sinh($\alpha\sigma$)]

$$\dot{\varepsilon}=1.363\times10^{17}[\sinh(0.01699\sigma)]^{5.526}\cdot\exp\left(-\frac{234510}{RT}\right) \tag{12}$$

Also, Zener−Hollomon parameter for as-quenched 7005 alloy can be represented as follows:

$$Z=\dot{\varepsilon}\exp\left(\frac{234.51}{RT}\right)=A[\sinh(\alpha\sigma)]^n= 1.363\times10^{17}[\sinh(0.01699\sigma)]^{5.526} \tag{13}$$

Based on Eq. (5), the flow stress constitutive equation of hot deformation for as-quenched 7005 alloy can also be expressed by Zener−Hollomon parameter as follows:

$$\sigma=58.858\ln\left\{\left(\frac{Z}{1.363\times10^{17}}\right)^{1/5.526}+\left[\left(\frac{Z}{1.363\times10^{17}}\right)^{2/5.526}+1\right]^{1/2}\right\} \tag{14}$$

A comparison between the experimental and calculated flow stress by Eq. (14) is carried out to verify the developed constitutive equation of as-quenched 7005 aluminum alloy, as shown in Table 1. In order to evaluate the accuracy of the developed constitutive equation, the error (e) between the calculated flow stress (σ_c) and measured flow stress (σ_m) can be calculated as

$$e=\frac{\sigma_c-\sigma_m}{\sigma_m}\times100\% \tag{15}$$

It can be easily found that, in the worst case, the mean error in the flow stress estimate is only 1.40% and standard deviation is 3.17%. The results indicate that the proposed deformation constitutive equation gives an accurate and precise estimate of the flow stress for as-quenched 7005 aluminum alloy.

Table 1 Comparison of calculated (σ_c) and measured (σ_m) flow stress

Strain rate/s^{-1}	Temperature/°C	σ_c/MPa	σ_m/MPa	Error analysis		
				Error/%	Mean/%	Standard deviation/%
0.5	250	192.738	197.235	−2.28	0.19	2.61
	300	136.013	132.597	2.58		
	350	93.575	91.678	2.07		
	400	61.175	60.240	1.55		
	450	44.787	46.159	−2.97		
0.05	250	171.366	176.132	−2.71	0.114	2.68
	300	108.199	105.539	2.52		
	350	72.593	71.087	2.12		
	400	45.957	45.268	1.52		
	450	34.267	35.283	−2.88		
0.005	250	144.056	146.918	−1.95	0.56	2.10
	300	86.190	84.370	2.16		
	350	52.932	51.656	2.47		
	400	32.364	31.862	1.58		
	450	26.406	26.797	−1.46		
0.0005	250	115.224	113.727	1.32	1.40	3.17
	300	58.759	56.919	3.23		
	350	39.633	37.867	4.66		
	400	22.640	22.306	1.50		
	450	17.096	17.755	−3.71		

3.3 Processing map and microstructural examination

In recent years, the processing maps, which were developed on the basis of the "Dynamic Materials Model" by PRASAD et al [18], have been developed to identify the deformation temperature−strain rate window for hot working and optimize the hot working processes of metals [19−23]. Briefly, the work-piece undergoing hot deformation is considered to be a dissipator of power and total power dissipated instantaneously is given by

$$P=\int_0^{\dot{\varepsilon}}\sigma \mathrm{d}\dot{\varepsilon}+\int_0^{\sigma}\dot{\varepsilon}\mathrm{d}\sigma=G+J \tag{16}$$

where σ is the flow stress and $\dot{\varepsilon}$ is the strain rate. The first integral is called G content representing deformation heat and the second one is called J co-content representing microstructural dissipation.

For the given strain and deformation temperature, the flow stress can be expressed as

$$\sigma=K\dot{\varepsilon}^{m} \tag{17}$$

where K is a material constant; m is the strain rate sensitivity used for partitioning the power into G content and J co-content:

$$m=\frac{\mathrm{d}J}{\mathrm{d}G}=\frac{\partial(\lg\sigma)}{\partial(\lg\dot{\varepsilon})} \tag{18}$$

J co-content can be expressed as

$$J=\int_0^{\sigma}\dot{\varepsilon}\mathrm{d}\sigma=\frac{m}{m+1}\sigma\dot{\varepsilon} \tag{19}$$

The efficiency of power dissipation occurring through microstructural changes during deformation is derived by comparing the non-liner power occurring instantaneously in the work-piece with a liner dissipater (m=1) and is given by

$$\eta=\frac{\Delta J/\Delta P}{(\Delta J/\Delta P)_{\text{linear}}}=\frac{m/(m+1)}{1/2}=\frac{2m}{m+1} \tag{20}$$

The value of m can be obtained by differentiating the third order polynomial fitting line of $\lg\dot{\varepsilon}-\lg\sigma$ plot. The variation of efficiency of power dissipation (η) with temperature and strain rate gives the power dissipation map which is generally viewed as an iso-efficiency contour map and exhibits different domains correlated with the specific microstructural mechanisms.

Further, using the principle of the maximum rate of the entropy of production, a continuum criterion for the occurrence of flow instabilities is defined in terms of the instability parameter $\xi(\dot{\varepsilon})$:

$$\xi(\dot{\varepsilon})=\frac{\partial\lg[m/(m+1)]}{\partial\lg\dot{\varepsilon}}+m\le 0 \tag{21}$$

The variation of the instability parameter as a function of temperature and strain rate represents an instability map which delineates regimes of instability where $\xi(\dot{\varepsilon})$ is negative. A processing map can be constructed by superimposing the instability map over the power dissipation map. The processing maps help depicting some typical microstructural deformation mechanisms, avoiding flow instabilities, optimizing deformation process parameter and obtaining favorable microstructures and mechanical properties.

In the present study, the processing maps obtained by superimposing the instability maps on the power dissipation maps at the strains of 0.1, 0.3 and 0.5 are shown in Fig. 8. The contour numbers indicate the

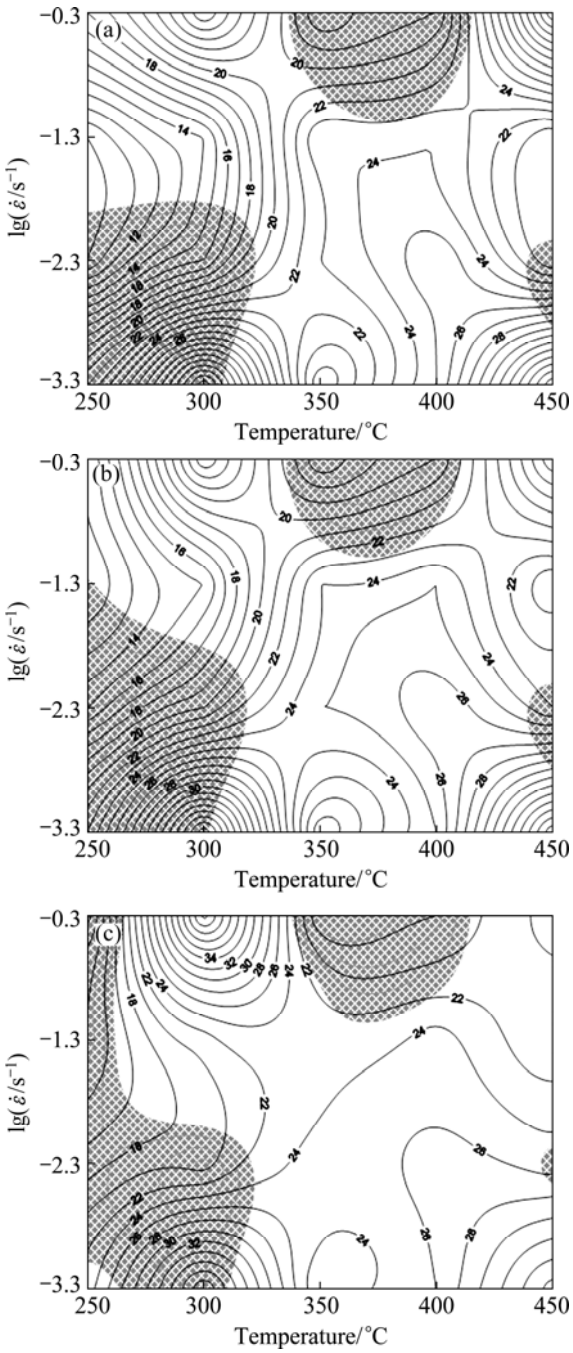

Fig. 8 Processing map of as-quenched 7005 alloy under strains of 0.1 (a), 0.3 (b) and 0.5 (c)

efficiency of power dissipation (η), and the shaded regions represent the instability regions. From Fig. 8, it can be found that the shaded areas denoting the instability domains increase with the increase of strain. Meanwhile, the shapes of the processing maps are similar for the strains of 0.1 and 0.3, However, there exist obvious differences in the shape of the processing maps when the strain is 0.5, which is probably caused by the occurrence of dynamic recrystallization under these deformation conditions.

As can be seen in Fig. 8(c), there are three typical peak efficiency domains in the processing map. The first domain is the deformation temperature ranging from 270 °C to 340 °C and strain rate ranging from 0.05 s^{-1} to 0.5 s^{-1}, with a peak efficiency of 44% occurring at about 300 °C, 0.5 s^{-1}. The second domain is the deformation temperature ranging from 325 °C to 340 °C and strain rate ranging up to 0.003 s^{-1}. The maximum efficiency in this domain is 34%. This domain is not suitable for the bulk metal processing because this region is very close to the instable domain and rather narrow. The third domain is the deformation temperature ranging from 380 °C to 450 °C and strain rate ranging from 0.0005 s^{-1} to 0.004 s^{-1} with a peak efficiency of 38% occurring at about 450 °C, 0.0005 s^{-1}. It is widely recognized that the high peak power dissipation efficiency is often associated with dynamic recrystallization or superplasticity. According to results by LIN et al [4], the efficiency of power dissipation for occurrence of superplasticity is beyond 60%. The peak efficiency for as-quenched 7005 alloy is not more than 45%. Hence, superplasticity may not occur in these domains. The microstructures of specimens deformed in the first and the third domains are shown in Figs. 9(a) and (b), respectively, which correspond to deformation conditions of 300 °C, 0.5 s^{-1} and 450 °C, 0.0005 s^{-1}, respectively. The microstructures exhibit some ideal features: the grain size is fine compared with initial grain size (about 400 μm) and the deformed grains are almost equiaxed, the grains boundaries exhibit wavy and irregular in nature [24], indicating that the domains observed present dynamic recrystallization. Generally, dynamic recrystallization is a beneficial process in hot deformation since it can provide stable flow and good workability to material by simultaneous softening and making the microstructure reconstituted. Further observation indicates that the dynamic recrystallization grains become coarse due to the higher deformation temperature and the lower strain rate in the third domain, which has a negative effect on the mechanical properties for the as-quenched 7005 alloy. Therefore, the third domain is not the optimum hot working domain. In conclusion, the processing map exhibits that the optimum hot working domain for the reasonable dynamic recrystallization (the average grain diameter is about 30 μm) is the temperature range of 270−340 °C and strain rate range of 0.05−0.5 s^{-1} with a peak efficiency of 44%.

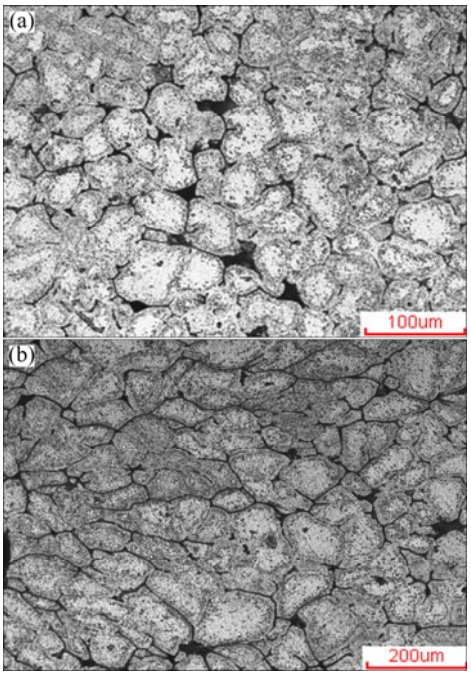

Fig. 9 Microstructures of as-quenched 7005 aluminum alloy deformed at 300 °C, 0.5 s^{-1} (a), and 450 °C, 0.0005 s^{-1} (b)

Meanwhile, the shaded domain in Fig. 8(c) represents the regimes of flow instabilities. For the domain under the low deformation temperature (250−270 °C) and high strain rate (0.05−0.5 s^{-1}), it is 'safe' when the strain is not more than 0.3, but it becomes instability when the strain ranges up to 0.5, resulting from the formation of adiabatic shear bands or flow localization [3,25,26]. The optical micrograph corresponding to deformation condition of 250 °C and 0.5 s^{-1} is shown in Fig. 10(a), in which adiabatic shear bands can be observed at an angle of 45° to the compressive axis. At the higher strain rates, adiabatic deformation heat generated during hot working is not conducted due to insufficient time and low thermal conductivity, inducing highly localized flow along the maximum shear stress plane [27], which is the process of adiabatic shear bands formation. Meanwhile, the flow localization occurs in another shaded domain in the processing map in the range of 325−425 °C and 0.05−0.5 s^{-1}, and the optical micrograph corresponding to the deformation condition of 400 °C and 0.5 s^{-1} is shown in Fig. 10(b). Generally, the instability domains with the formation of adiabatic shear bands or flow localization may result in cracking along the macroscopic shear planes [28]. Hence, these domains should be avoided during hot working.

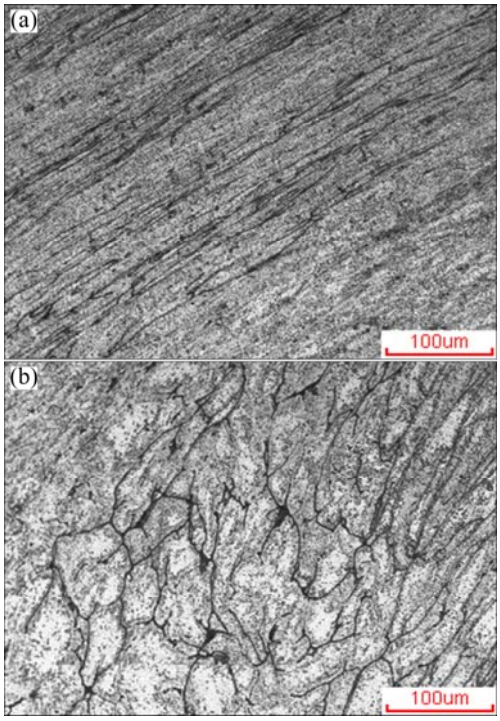

Fig. 10 Microstructures occurring in instability domain of as-quenched 7005 aluminum alloy: (a) Adiabatic shear bands at 250 °C, 0.5 s^{-1}; (b) Flow localization at 400 °C, 0.5 s^{-1}

4 Conclusions

1) The flow stress of as-quenched 7005 aluminum alloy is evidently affected by deformation temperature and strain rate, namely, the flow stress increases with the increase of strain rate and the decrease of the deformation temperature, which can be represented by a Zener−Hollomon parameter in an exponent-type equation.

2) A constitutive equation for as-quenched 7005 aluminum alloy was established by using a hyperbolic sine equation. The flow stress at a true strain of 0.5 was analyzed using this constitutive equation, and the value of deformation activation (Q) was obtained and it is 234.51 kJ/mol. The comparisons between the calculated and experimental results indicate that the proposed deformation constitutive equation can give an accurate estimate of the flow stress for as-quenched 7005 aluminum alloy.

3) The processing maps and microstructural examination revealed that the optimum hot working domain for as-quenched 7005 alloy is the temperature range of 270−340 °C and strain rate range of 0.05−0.5 s^{-1} with the reasonable dynamic recrystallization. Moreover, the alloy exhibited flow instability at high strain rates, which is associated with the formation of adiabatic shear bands and flow localization.

References

[1] WANG X Y, HU H E, XIA J C. Effect of deformation condition on plastic anisotropy of as-rolled 7050 aluminum alloy plate [J]. Materials Science Engineering A, 2009, 515(1−2): 1−9.

[2] WILLIAMS J C, STARKE E A Jr. Progress in structural materials for aerospace systems1 [J]. Acta Materialia, 2003, 51(19): 5775−5799.

[3] RAJAMUTHAMILSELVAN M, RAMANATHAN S. Hot deformation behaviour of 7075 alloy [J]. Journal of Alloys and Compounds, 2011, 509(3): 948−952.

[4] LIN Y C, LI L T, XIA Y C, JIANG Y Q. Hot deformation and processing map of a typical Al−Zn−Mg−Cu alloy [J]. Journal of Alloys and Compounds, 2013, 550: 438−445.

[5] JIN N P, ZHANG H, HAN Y, WU W X, CHEN J H. Hot deformation behavior of 7150 aluminum alloy during compression at elevated temperature [J]. Materials Characterization, 2009, 60(6): 530−536.

[6] ZHEN L, HU H, WANG X Y, ZHANG B Y, SHAO W Z. Distribution characterization of boundary misorientation angle of 7050 aluminum alloy after high-temperature compression [J]. Journal of Materials Processing Technology, 2009, 209(2): 754−761.

[7] PRASAD Y V R K, SESHACHARYULU T. Processing maps for hot working of titanium alloys [J]. Materials Science and Engineering A, 1998, 243(1−2): 82−88.

[8] McQUEEN H J, IMBERT C A C. Dynamic recrystallization: Plasticity enhancing structural development [J]. Journal of Alloys and Compounds, 2004, 378(1−2): 35−43.

[9] LIN Y C, CHEN M S, ZHONG J. Effect of temperature and strain rate on the compressive deformation behavior of 42CrMo steel [J]. Journal of Materials Processing Technology, 2008, 205(1−3): 308−315.

[10] LEE W S, LIN M T. The effects of strain rate and temperature on the compressive deformation behaviour of Ti−6Al−4V alloy [J]. Journal of Materials Processing Technology, 1997, 71(2): 235−246.

[11] YANG X W, LAI Z H, ZHU J C, LIU Y, HE D. Hot compressive deformation behavior of the as-quenched A357 aluminum alloy [J]. Materials Science and Engineering B, 2012, 177(19): 1721−1725.

[12] GUAN Shao-kang, WU Li-hong, WANG Li-guo. Flow stress and microstructure evolution of semi-continuous casting AZ70 Mg-alloy during hot compression deformation [J]. Transactions of Nonferrous Metals Society of China, 2008, 18(2): 315−320.

[13] MA Ming-long, ZHANG Kui, LI Xing-gang, LI Yong-jun, ZHANG Kang. Hot deformation behavior of rare earth magnesium alloy without pre-homogenization treatment [J]. Transactions of Nonferrous Metals Society of China, 2008, 18(S1): s132−s139.

[14] DUAN Yuan-pei, LI Ping, XUE Ke-min, ZHANG Qing, WANG Xiao-xi. Flow behavior and microstructure evolution of TB8 alloy during hot deformation process [J]. Transactions of Nonferrous Metals Society of China, 2007, 17(6): 1199−1204.

[15] SHI H, MCLAREN A J, SELLARS C M, SHAHANI R, BOLINGBROKE R. Constitutive equations for high temperature flow stress of aluminum alloys [J]. Materials Science and Technology, 1997, 13(3): 210−216.

[16] MAHMUDI R, ROUMINA R, RAEISINIA B. Investigation of stress exponent in the power-law creep of Pb−Sb alloys [J]. Materials Science and Engineering A, 2004, 382(1−2): 15−22.

[17] SRIVASTAVA V C, JINDAL V, UHLENWINKEL V, BAUCKHAGE K. Hot-deformation behaviour of spray-formed 2014 Al+SiCp metal matrix composites [J]. Materials Science and Engineering A, 2008, 477(1−2): 86−95.

[18] PRASAD Y V R K, SASIDHARA S, SIKKA V K. Characterization

of mechanisms of hot deformation of as-cast nickel aluminide alloy [J]. Intermetallics, 2000, 8(9−11): 987−995.

[19] ABBASI S M, MOMENI A. Hot working behavior of Fe−29Ni−17Co analyzed by mechanical testing and processing map [J]. Materials Science and Engineering A, 2012, 552: 330−335.

[20] MOMENI A, DEHGHANI K. Hot working behavior of 2205 austenite-ferrite duplex stainless steel characterized by constitutive equations and processing maps [J]. Materials Science and Engineering A, 2011, 528(3): 1448−1454.

[21] RAMANATHAN S, KARTHIKEYAN R, GUPTA M. Development of processing maps for Al/SiCp composite using fuzzy logic [J]. Journal of Materials Processing Technology, 2007, 183(1): 104−110.

[22] SAMANTARAY D, MANDAL S, BHADURI A K. Characterization of deformation instability in modified 9Cr−1Mo steel during thermo-mechanical processing [J]. Materials and Design, 2011, 32(2): 716−722.

[23] HUANG Guang-sheng, WANG Ling-yun, CHEN Hua, HUANG Guang-jie, ZHANG Suo-quan. Hot deformation and processing maps of 2618 aluminum alloy [J]. The Chinese Journal of Nonferrous Metals, 2005, 15(5): 763−767. (in Chinese)

[24] WANG C Y, WANG X J, CHANG H, WU K, ZHENG M Y. Processing maps for hot working of ZK60 magnesium alloy [J]. Materials Science and Engineering A, 2007, 464(1−2): 52−58.

[25] ANBUSELVAN S, RAMANATHAN S. Hot deformation and processing maps of extruded ZE41A magnesium alloy [J]. Materials and Design, 2010, 31(5): 2319−2323.

[26] RAO K P, PRASAD Y V R K, SURESH K, HORT N, KAINER K U. Hot deformation behavior of Mg−2Sn−2Ca alloy in as-cast condition and after homogenization [J]. Materials Science and Engineering A, 2012, 552: 444−450.

[27] VENUGOPAL S, VENUGOPAL P, MANNAN S L. Optimisation of cold and warm workability of commercially pure titanium using dynamic materials model (DMM) instability maps [J]. Journal of Materials Processing Technology, 2008, 202(1−3): 201−215.

[28] ANBUSELVAN S, RAMANATHAN S. Hot workability of as-cast and extruded ZE41A magnesium alloy using processing maps [J]. Transactions of Nonferrous Metals Society of China, 2011, 21(2): 257−264.

淬火态 7005 铝合金的热变形行为

王明亮，金培鹏，王金辉，韩 丽

青海大学 机械工程学院，青海省新型轻合金重点实验室，西宁 810016

摘 要：在 Gleeble−1500 热模拟仪上进行热压缩实验，研究在变形温度 250~450 ℃、应变速率 0.0005~0.5 s^{-1} 时淬火状态下的 7005 铝合金的热变形行为。实验结果表明：淬火状态 7005 合金的流变应力受变形温度和应变速率的双重影响，热变形过程中的流变应力可用 Zener−Hollomon 参数的指数型方程表示。通过比较本构方程计算出的流变应力和实验测量的流变应力发现预测结果和实验结果有很好的相符性。基于动态材料模型，在真应变为 0.1、0.3 和 0.5 处构建了淬火状态下的 7005 铝合金的热加工图。通过加工图分析及微观组织观察发现合金的最优热加工区域为：270~340 ℃，0.05~0.5 s^{-1}，在该区域内变形时合金发生了合理的动态再结晶行为。合金的流变不稳定性与绝热剪切带以及局部流变的产生有关。因此，为获取满意的性能，在热加工时应避开这些不稳定的区域。

关键词：7005 合金；热压缩变形；本构方程；加工图

(Edited by Hua YANG)